

Quantum computing in neural networks

P. GRALEWICZ

Department of Theoretical Physics, University of Łódź, Pomorska 149/153, 90-236, Łódź, Poland

Abstract

According to the statistical interpretation of quantum theory, quantum computers form a distinguished class of probabilistic machines (PMs) by encoding n qubits in $2n$ pbits (random binary variables). This raises the possibility of a large-scale quantum computing using PMs, especially with neural networks which have the innate capability for probabilistic information processing. Restricting ourselves to a particular model, we construct and numerically examine the performance of neural circuits implementing universal quantum gates. A discussion on the physiological plausibility of proposed coding scheme is also provided.

1 Introduction

Neural networks are naturally evolved systems for information processing. Despite decades of experimental and theoretical research, there is no agreement upon the information encoding employed by these circuits – the problem of what exactly is being communicated *via* seemingly chaotic spike trains is still largely open [1]. Advancement in understanding of this neural language is obstructed by variety of cell types, working conditions and molecular factors to be taken into account [2]. Generally accepted schemes, the *rate code* and the *phase code*, may turn out to be only the first two in a sequence of progressively more intricate codes, where higher order correlations within cellular complexes are utilized.

Quantum information science, on the other hand, had matured over the last two decades making significant contributions to both information theory and quantum mechanics (QM). The latter, having historical roots in particle physics, is still often identified with the micro-world. Yet, there is nothing in the mathematical foundations of QM which could justify that point of view. In fact, apart from that microscopic realizations, quantum theory has found many avatars, from mechanical [3], linguistic [4], purely geometric [5], to statistical [6–9]. In this article, that last, widely accepted interpretation, is being used to study the feasibility of a hypothesis that spike trains may actually encode for quantum states.

Such hypothesis appears particularly attractive in that the Nature is notorious in repeating itself at various scales, and if quantum computing (QC) proves to be practical, it would be rather surprising if one could not find it implemented at a higher level. From this point of view neural networks are the obvious candidates for such implementations. By examining two neural circuits, designed to perform quantum operations (1-qubit rotations, and 2-qubit CNOT gate), we demonstrate the feasibility of our hypothesis within the limits of a simple model. Although quantum registers are realized efficiently with just two neurons per qubit, the major costs are in the processing of information carried by the spike trains. The simulations provided are intended to empha-

size the amount of these resources as well as the functionality required for implementation.

We begin with a short review of the formalism which allows for the identification of pairs of spiking neurons with qubits. In Section 3 a reduced model of neural network is described, which in Sec. 4 is further used as a basis for construction of quantum gates. The results of simulations, in terms of achieved fidelity and coherence, are promising enough to look toward more realistic implementations. We touch briefly on these issues in the last section.

2 Manipulation of quantum states embedded in probabilistic space

The operational approach to quantum mechanics, through the formalism of positive operator-valued measures (POVMs), allows one to express the states of a quantum system defined in a finite-dimensional Hilbert space \mathcal{H} , in terms of probability distributions. If the dimension is $d := \dim \mathcal{H}$, then a generic density matrix $\hat{\rho}$ representing the state has $d^2 - 1$ degrees of freedom (DOFs). A distribution obtained through particular POVM has length d^2 , and – due to normalization constraint – the same number of DOFs as the density matrix [8]. For n -qubit states, this distribution can be associated with joint probability of $2n$ binary random variables¹.

Let $\hat{\rho}$ be a generic density matrix of a 1-qubit state, which using summation convention, we write as

$$\hat{\rho} := \varrho^\mu \hat{\sigma}_\mu = \begin{pmatrix} \frac{1}{2} + \varrho^3 & \varrho^1 + i\varrho^2 \\ \varrho^1 - i\varrho^2 & \frac{1}{2} - \varrho^3 \end{pmatrix},$$

where $\hat{\sigma}_0 = \mathbb{1}$, $\hat{\sigma}_{1,2,3}$ are the Pauli matrices, $\varrho^0 \equiv \frac{1}{2}$, and $\varrho^1, \varrho^2, \varrho^3 \in [-\frac{1}{2}, \frac{1}{2}]$ are the three real coordinates of a Bloch vector. Let $\{\hat{A}^z\}$ be a normalized 4-element positive operator-valued measure

$$\sum_z \hat{A}^z = \mathbb{1}, \quad z = 0, \dots, 3. \quad (1)$$

¹This is in close analogy to complex numbers which extend the reals, and at the same time are embeddable in a real vector space of doubled dimension equipped with complex structure.

Typically, one associates such a POVM with the Pauli basis, that is

$$\hat{A}^z := A^z_{\mu} \hat{\sigma}^{\mu} = \frac{1}{2} \mathbb{1} + A^z_i \hat{\sigma}^i, \quad i = 1, \dots, 3.$$

where $A^z_0 \equiv \frac{1}{2}$, and $\hat{\sigma}^{\mu} := \hat{\sigma}^{\mu\dagger} = \hat{\sigma}_{\mu}$, is the basis dual with respect to the scalar product $\langle \hat{\sigma}^{\mu}, \hat{\sigma}_{\nu} \rangle := \frac{1}{2} \text{tr}[\hat{\sigma}^{\mu} \hat{\sigma}_{\nu}] = \delta^{\mu}_{\nu}$. Although not a strict necessity, it is reasonable to assume the same POVM for all n qubits within a register, and consequently take the entire POVM as a n -fold tensor product

$$\hat{A}^{z_1 \dots z_n} := \hat{A}^{z_1} \otimes \dots \otimes \hat{A}^{z_n}.$$

This leads to the following distribution

$$p^{z_1 \dots z_n} := \langle \hat{A}^{z_1 \dots z_n}, \hat{\rho} \rangle = 2^{-2n} + A^{z_1}_{i_1} \dots A^{z_n}_{i_n} \varrho^{i_1 \dots i_n},$$

$$\sum_{z_1 \dots z_n} p^{z_1 \dots z_n} = 1.$$

Introducing the event basis $\{\hat{e}_z\}$, the transformation can concisely be written as

$$\hat{p} = A \hat{\rho}, \quad (2)$$

where

$$\hat{p} = p^{z_1 \dots z_n} \hat{e}_{z_1} \otimes \dots \otimes \hat{e}_{z_n},$$

$$A = A^{z_1}_{\mu_1} \dots A^{z_n}_{\mu_n} \hat{e}_{z_1} \otimes \dots \otimes \hat{e}_{z_n} \otimes \hat{\sigma}^{\mu_1} \otimes \dots \otimes \hat{\sigma}^{\mu_n}.$$

Conversely, if $\{\hat{A}^z\}$, are linearly independent, then one can invert the relation (2) and take the distribution \hat{p} as an equivalent representation of the quantum state $\hat{\rho} = A^{-1} \hat{p}$.

A unitary transformation $U \in \text{U}(2^n)$ of the state is a linear operator² $L \in 1 \oplus \text{SO}(2^{2n} - 1)$

$$\hat{\rho} \mapsto U^{\dagger} \hat{\rho} U = L \hat{\rho},$$

with elements

$$L^{\mu_1 \dots \mu_n}_{\nu_1 \dots \nu_n} = \langle \hat{\sigma}^{\mu_1} \otimes \dots \otimes \hat{\sigma}^{\mu_n}, U^{\dagger} \hat{\sigma}_{\nu_1} \otimes \dots \otimes \hat{\sigma}_{\nu_n} U \rangle. \quad (3)$$

After transformation of the basis $A^{-1} : \{\hat{\sigma}_{\mu}\} \rightarrow \{\hat{e}_z\}$ one has the same operation acting on probability distribution

$$\hat{p} \mapsto (ALA^{-1}) \hat{p}. \quad (4)$$

There is, however, an important difference between the linear dynamics of Eq. (4) and Markovian transitions usually considered in association with stochastic evolution: Denote by Ω^{2n} the space of joint probability distributions of $2n$ pbits. Since the operator ALA^{-1} is by definition invertible, it follows that, in general, it is not a positive one, hence only a subset of Ω^{2n} will be mapped

²Note, that the embedding allows to consider a wider range of isometries to be implemented, not only the ones corresponding to unitary operations. For instance the 1-qubit antipode (unfortunately also called the quantum universal-NOT) can only be approximated in unitary QM [10, 11]. In probabilistic approach one can realize it exactly.

back into itself. We denote this subset – the (closure of) positive domain of quantum operators – by

$$\overline{\Omega_+^{2n}} := \{\hat{p} \in \Omega^{2n} \mid ALA^{-1} \hat{p} \in \Omega^{2n}\}.$$

This is simply the image of all quantum states under the POVM A . The boundary $\Omega_0^{2n} := \partial \overline{\Omega_+^{2n}}$, which is the image of the Bloch sphere in Ω^{2n} contains pure states, while its interior $\Omega_+^{2n} := \overline{\Omega_+^{2n}} \setminus \Omega_0^{2n}$ is the subset of mixed states. All remaining distributions $\Omega_-^{2n} := \Omega^{2n} \setminus \overline{\Omega_+^{2n}}$ are mapped by A^{-1} to the exterior of the Bloch sphere. Therefore, the POVM partitions the set of possible distributions into three disjoint subsets:

$$\begin{array}{ll} \Omega_0^{2n} & \text{– pure quantum states} \\ \Omega_+^{2n} = \text{int } \Omega_0^{2n} & \text{– mixed/decohered states} \\ \Omega_-^{2n} = \text{ext } \Omega_0^{2n} & \text{– overcohered states} \end{array}$$

To explain the term *overcohered* used above, let us take a closer look at the limitations imposed by the POVM on distributions in $\overline{\Omega_+^{2n}}$. Positivity of A implies, that the probabilities are bound by

$$p^{z_1 \dots z_n} \leq 2 \langle p \rangle = 2(A^z_0 \varrho^0)^n = 2^{1-2n}.$$

Furthermore, if, as we assume, A is non-degenerate, then for any quantum state only one of the elements $\{p^{z_1 \dots z_n}\}$ can either vanish, or reach the maximal value $2 \langle p \rangle$. This means, that there is a non-zero lower bound on the entropy of distributions in $\overline{\Omega_+^{2n}}$, and hence no distribution with certain outcome can represent a quantum state. Moreover, all single-pbit marginals are non-vanishing.

A quantitative characterization of the *coherence* can be given by the radius of the state's Bloch vector. The metric $g : \Omega^{2n} \times \Omega^{2n} \rightarrow \mathbb{R}$ induced by the POVM on the distribution space permits to obtain this radius directly for an arbitrary $\hat{p} \in \Omega^{2n}$. Let $\hat{p}_1, \hat{p}_2 \in \overline{\Omega_+^{2n}}$, and $\hat{\rho}_1, \hat{\rho}_2$ be corresponding quantum states. Then g is given by

$$g(\hat{p}_1, \hat{p}_2) := \text{tr}[\hat{\rho}_1^{\dagger} \hat{\rho}_2] = (A^{-1} \hat{p}_1)^{\dagger} \cdot (A^{-1} \hat{p}_2).$$

Because this is a bilinear map with coefficients independent of \hat{p}_1, \hat{p}_2 , one is free to extend its domain onto the entire space Ω^{2n} . Since $A^0_{\mu} = \frac{1}{2}$, the radius is

$$r^2 := \|\vec{\rho}\|^2 = 2^{-n} g(\hat{p}, \hat{p}) - 2^{2n}.$$

In particular, for a pure state

$$r_{\text{pure}}^2 = 2^{-n} (1 - 2^{-n}),$$

and the Bloch radius of any mixed state is always bound by $r < r_{\text{pure}}$. The ratio

$$R := \frac{r}{r_{\text{pure}}}, \quad (5)$$

can be adopted for a measure of coherence – ranging from $R = 0$ for maximally decohered state $\hat{\rho} = 2^{-n}\mathbb{1}$, through $R = 1$ for any pure $\hat{\rho} = \hat{\rho}^2$, and beyond $R > 1$ for all overcohered ones.

In order to quantify the performance of circuits considered latter in this article, we will also employ another, independent measure by which one can estimate the angular disparity between expected and obtained states. The *fidelity* or normalized overlap between $\hat{p}, \hat{q} \in \Omega^{2^n}$ is defined here as

$$F := \frac{g(\hat{p}, \hat{q})}{\sqrt{g(\hat{p}, \hat{p})} \sqrt{g(\hat{q}, \hat{q})}}.$$

We choose fidelity as a commonly adopted measure, for the purpose of comparison, notwithstanding direct estimate of the unitary error between the desired pure state $\hat{p} \in \Omega_0^{2^n}$ and obtained distribution $\hat{q} \in \Omega^{2^n}$, which is readily computable:

$$\alpha = \arccos \left(\frac{g(\hat{p}, \hat{q}) - 2^{-n}}{r(\hat{q}) \sqrt{2^n - 1}} \right).$$

The two quantities α and F , are nevertheless dependent.

3 A toy-model neural-network

The information in neural networks is carried by spike trains, which after appropriate discretization can be transformed to binary strings. The model network described in this section is a much simplified version of what usually is considered realistic – the purpose of such reduction is to retain only the essential features. Consistently with discretization of transmitted signals, the model operates in explicitly step-wise manner, instead of continuous-time evolution. Likewise, the delays effected along the inter-neuron paths are also taken to be integers.

Let $\mathcal{G} = (\mathcal{V}, \mathcal{E})$, be a multiply-connected digraph, where $\mathcal{V} = \{\hat{v}_i\}$ is the vertex basis of neurons, (we shall also write \mathcal{V}_N to explicit the number N of vertices involved) and $\mathcal{E} = \mathcal{V} \otimes \mathcal{V} \otimes \mathbb{N}$ is the basis of edges, that is the possible synaptic connections. The actual couplings between i^{th} and j^{th} neuron are set by the weights $W^i_{j,s}$ where $s \in \mathbb{N}$ enumerates the delays introduced along multiple edges. For each vertex we define two variables: the binary *output state* $X^i \in \{0, 1\}$, and the *residual potential* $u^i \in \mathbb{R}$.

We adopt the discrete *integrate-and-fire* scheme for the dynamics of this network. In each time step the potential is first updated by accumulating the incoming signals

$$u^{i,t-1} \mapsto u_*^{it} := u^{i,t-1} + \sum_j W^i_{j,s} X^{j,t-s}$$

where the summation runs over connected vertices (j) and edge delays ($s \geq 1$). Subsequent spike generation ($X^{it} = 1$) occurs with probability $P(u_*^{it})$, where $P : \mathbb{R} \rightarrow [0, 1]$, is a ‘noisy’ activation function with firing threshold fixed at $u_{\text{thr}} = \frac{1}{2}$. Its actual form used in

simulations is given by

$$P(u_*) := \frac{1}{2} \left(1 + \operatorname{erf} \frac{u_* - u_{\text{thr}}}{\sigma} \right),$$

where $\sigma \geq 0$ is a global control parameter characterizing the noise standard deviation (SD). In particular, in the limit $\sigma \rightarrow 0$ the spikes are produced deterministically, as P becomes a step-function. The excited state u_*^{it} is eventually reduced by release of a spike (refractory potential), and further quenched with a bound, nonlinear map S

$$u_*^{it} \mapsto u^{it} = S(u_*^{it} - X^{it}).$$

We assume S to have an attractive fixed point at the origin (the resting potential), $\forall u : \lim_{t \rightarrow \infty} S^t(u) = 0$, to be linear in its neighborhood $S'(0) = 1$, and having finite, but non-zero asymptotes $|S(\pm\infty)| < \infty$. The motivation for introduction of this mapping is twofold: First, the physiological mechanisms of signal transmission imply existence of *saturations* in both positive and negative direction. The cell can be depolarized or hyperpolarized through synaptic channels only to certain extent, and adding more excitatory or inhibitory connections will not have a significant effect. Second, the reason to have $u = 0$ for an attractive fixed point, is to imitate the ‘leaky’ integration scenario, by which in the absence of input the potential returns back to its resting point. In the simulations this function was taken to be a simple, skew-symmetric mapping

$$S(u) := \gamma \tanh \frac{u}{\gamma}, \quad \gamma \geq 0.$$

Here, the asymptotes are $S(\pm\infty) = \pm\gamma$, therefore we call γ the ‘saturation parameter’. If we assume, that the neuron is left without input and some residual u , so that no spikes are generated, then the potential u will decay sub-exponentially in time, as

$$u \mapsto S^t(u) \xrightarrow[t \gg 1]{} \frac{\gamma u}{\sqrt{\gamma^2 + \frac{2}{3} t u^2}},$$

where S^t means t -fold composition. In the limit $\gamma \rightarrow 0$, the residual potential is reset to zero after each cycle, and this situation can be associated with time steps longer than the total refractory time (~ 20 ms), within which the cell relaxes to its resting point. If $\gamma > 0$, then the probability of a consecutive spike is modified by the residual potential: The cell is within the *relative* refractory period, when the the potassium channels are still open, but the sodium gates are already reverted to their normal state. This mode corresponds to time steps of order ~ 5 ms. Shorter times are generally unrealistic due to high suppression of spike generation during the *absolute* refractory period, when the sodium channels are closed.

The choice of a specific value of γ is therefore indirectly related to the time scale, and consequently to the discretization window of action potentials. If this window is too short, the discretization becomes ambiguous

and the model breaks down – this is another reason not to consider high saturation values.

The qualitative behavior of the above model is best understood by analyzing single neuron at the limits of the two control parameters σ , and γ . Assume the cell is fed with a stimulus at a constant frequency $\nu_{\text{in}} \in [0, 1]$, and consider at first the noiseless regime $\sigma = 0$. If $\gamma = 0$, then the only memory of past input values is stored in delayed connections. The cell fires only if the value of the convolution $W_{js}X^{j,t-s}$ exceeds the threshold u_{thr} . Such neurons acts like a high-pass filter and its firing rate is $\nu_{\text{out}} = P(\nu_{\text{in}} \sum_{s,j} W_{js})$. By increasing the noise SD σ , the shape of this filtering function changes along with the spiking probability P , nevertheless it never becomes close to an ideal multiplier – the response is always non-linear.

If $\gamma \rightarrow \infty$ the cell accumulates and ‘remembers’ the residual value of convolution left over after subtraction of generated spikes. This makes it into a perfect multiplier with spike rate $\nu_{\text{out}} = \nu_{\text{in}} \sum_{s,j} W_{js}$. Raising σ above zero does not change this average response, but the determinism initially apparent in the spike patterns is gradually being washed away.

In between of these two regimes, lies a surprisingly complex area of fractal-spaced frequency thresholds and output patterns, particularly conspicuous at $\sigma = 0$ and $\nu_{\text{in}} = 1$. Presence of these features, found in many non-linear deterministic systems do not critically depend on the specific shape of the function S .

4 Implementation of universal quantum gates

According to the discussion provided in section 2, one needs $2n$ random binary variables to implement an n -qubit register. In our model of the neural network, these variables are identified with discretized spikes registered at $2n$ network sites. The question we set up to address in this section is, whether there are circuits which can implement state-independent rotations of the joint probability distributions, that is – quantum gates.

The set of gates universal for quantum computation [12] includes the whole algebra of 1-qubit rotations, and an arbitrary 2-qubit entangling gate, typically chosen to be the CNOT (controlled-NOT). Although probabilistic encoding of qubits is efficient (*i.e.* linear in n), manipulation of their 2^{2n} degrees of freedom (DOFs), by definition requires exponential amount of resources. From this perspective the construction of circuits described below should appear at least conceptually straightforward: The space of binary functions over the vertices \mathcal{V}_{2n} is $\mathcal{V}_*^{2n} = \mathbb{Z}_{2n}$. We first embed an element $X^t = \{X^{it}\} \in \mathcal{V}_*^{2n}$ into

³From the point of view of state estimation, the optimal POVM is a conformal transformation, which maps the Bloch sphere into a sphere inscribed in the standard simplex of $\mathbb{R}^{2^{2n}}$. Thanks to the many symmetries of such geometric configuration, some of the rotations are expressible as permutations of the simplex’ vertices and can be implemented with high efficiency. In the case of A given by Eq. (6), the permutation (00, 10)(01, 11) corresponds to the 1-qubit NOT gate. With a different POVM one can bring the Hadamard’s gate H to a permutation, therefore if an algorithm relies on frequent applications of this operation, that could be a preferred choice.

Ω^{2n} , then apply the gate $G := ALA^{-1}$, and finally project the result back onto \mathcal{V}_*^{2n} . The entire quantum gate transforming one set of spike trains X^t to another $Y^t \in \mathcal{V}_*^{2n}$, is then a composition

$$\Pi \circ G \circ \Pi^{-1} : X^t \mapsto Y^t,$$

where $\Pi^{-1} : \mathcal{V}_*^{2n} \rightarrow \Omega^{2n}$, and $\Pi \circ \Pi^{-1} = \text{id}_{\mathcal{V}_*^{2n}}$. The main problem in this approach is to construct a reliable projection Π , since any information loss during that operation will affect the quality of entire gate.

Concrete realization, requires also to decide upon particular POVM being used. It is possible to choose this transformation in such a way, that some of the gates will be significantly simplified, for instance acquiring convenient form of permutations. Our choice is dictated by the optimization of the CNOT gate, discussed latter in this section. This POVM is given by³

$$A^z_\mu := \frac{1}{2} \begin{pmatrix} 1 & -\frac{1}{\sqrt{3}} & -\frac{1}{\sqrt{3}} & -\frac{1}{\sqrt{3}} \\ 1 & \frac{1}{\sqrt{3}} & \frac{1}{\sqrt{3}} & -\frac{1}{\sqrt{3}} \\ 1 & -\frac{1}{\sqrt{3}} & \frac{1}{\sqrt{3}} & \frac{1}{\sqrt{3}} \\ 1 & \frac{1}{\sqrt{3}} & -\frac{1}{\sqrt{3}} & \frac{1}{\sqrt{3}} \end{pmatrix}. \quad (6)$$

4.1 Single-qubit gates

The neural circuit implementing arbitrary 1-qubit gate is presented in Fig. 1. The projection Π which transforms the ‘sparse’ code $\{X^{00'}, X^{01'}, X^{10'}, X^{11'}\} \in \Omega^2$ onto a ‘dense’ one $\{X^A, X^B\} \in \mathcal{V}_*^2$, is a linear mapping implemented with weights

$$W_\Pi = \begin{pmatrix} 0 & 0 & 1 & 1 \\ 0 & 1 & 0 & 1 \end{pmatrix}.$$

But its inverse, Π^{-1} is nonlinear and we realize this function, in a two-step linear-feedback operation. The first step requires, apart from the input signals, an additional supply of constant ‘current’ of units from the vertex \hat{v}_1 . The effect of such a coupling to unity on a cell is to alter its firing threshold. The weights of this part, effecting a linear injection from $\{X^A, X^B, 1\}$ to $\{X^{00}, X^{01}, X^{10}, X^{11}\}$ are

$$W_{\Pi^{-1}} = \begin{pmatrix} -1 & -1 & 1 \\ -1 & 1 & 0 \\ 1 & -1 & 0 \\ 1 & 1 & -1 \end{pmatrix}.$$

While the composition $W_\Pi W_{\Pi^{-1}} = \text{id}_{\mathcal{V}_*^2}$ as required, the reciprocal is not an identity and needs a rectifying feedback sent from the ‘winning’ neuron to its neighbors, in order to bring their residual potentials back to zero. Because of the one-step delay, this signal has to be adjusted

to match the attenuation already done by the function S . Hence the weight matrix of this rectification step is determined by

$$\begin{aligned} [W_{\text{rec}}]_{ij}^i &= -S([W_{\Pi^{-1}}W_{\Pi}]_{ij}^i - \delta_{ij}^i) \\ &= -S(-1)[\mathbb{1}_{\Omega^2} - W_{\Pi^{-1}}W_{\Pi}]_{ij}^i. \end{aligned} \quad (7)$$

Note, that for vanishing saturation parameter, this correction also disappears due to $S \equiv 0$.

In the absence of noise ($\sigma = 0$), the conversion Π^{-1} between dense and sparse coding is completely error-free. As σ increases, the imperfections start to appear in the form of either multiple, or ‘void’ spiking in the first hidden layer. Although we found the circuit to behave stably in these conditions, an improvement, in terms of both fidelity and coherence, can be achieved by adding a second, normalizing feedback (not shown explicitly in Fig. 1).

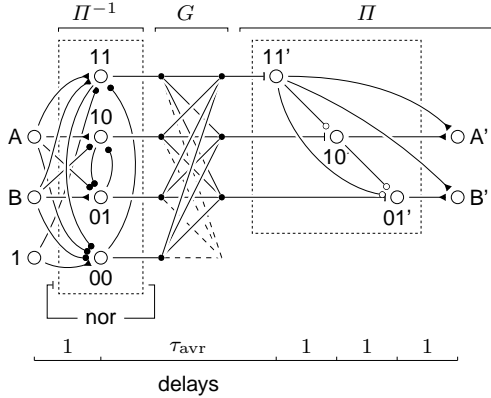


Figure 1 Schematic for the 1-qubit gate. The hidden nodes are drawn in inverted lexicographical order to avoid excessive entanglement of the graph. Explicit connections of the normalization (nor) feedback are omitted, to improve legibility. Inhibitory connections are marked with $(-\rightarrow)$, excitatory with $(-\leftarrow)$, and those capped with $(-|)$ depend on the applied gate G . The double connections $(-\circ)$ consist of inhibition followed by delayed and attenuated excitation. The transient time is $\tau_{\text{gate}} = 4 + \tau_{\text{avr}}$. Including the normalization feedback, and doubled gate connections ($\tau_{\text{avr}} = 2$), the circuit comprises 10 nodes, and 62 edges.

Normalizing feedbacks are commonly proposed for explanation of the observed behavior in cortical neurons [16, 17]. The main difference between these and our proposal is that while the former are multiplicative, this one acts additively. Its role is to adjust the residual potentials for the difference

$$1 - \sum_i X^i, \quad i = 00, 01, 10, 11.$$

Because we do not know which of the four neurons spiked mistakenly, the normalizing signal is sent evenly to all of them. Its strength is determined by the average excess of a signal encountered on a double-spike event:

$$\frac{1}{4} \sum_j [W_{\text{rec}}]_{ij}^i = -\frac{1}{4} S(-1).$$

The deficit, which happens upon lack of a single spike has the same magnitude but opposite sign. Therefore,

the weight matrix of this normalization reads

$$W_{\text{nor}} = -S(-1) \begin{pmatrix} -\frac{1}{4} & -\frac{1}{4} & -\frac{1}{4} & -\frac{1}{4} & 1 \\ -\frac{1}{4} & -\frac{1}{4} & -\frac{1}{4} & -\frac{1}{4} & 1 \\ -\frac{1}{4} & -\frac{1}{4} & -\frac{1}{4} & -\frac{1}{4} & 1 \\ -\frac{1}{4} & -\frac{1}{4} & -\frac{1}{4} & -\frac{1}{4} & 1 \end{pmatrix},$$

where the last column refers to the unit vertex \hat{v}_1 .

Making the embedding Π^{-1} robust is crucial for achieving correct projection Π . Multiple, or void events linearly projected *via* W_{Π} typically lead to a significant loss of coherence (although with less impact on fidelity). In order to compensate for these non-exclusive events, the spiking neuron sends a composite inhibitory signal down the hierarchy. This is implemented with double connections: the first transmits inhibitory signal at certain level η , and is followed by a delayed, excitatory one aimed at bringing the residual potential of target neuron back to its prior value. The full accomplishment of this goal is impossible with nonlinear function S – the value can only be fully restored in the linear limit $\gamma \rightarrow \infty$. Given the inhibitory coupling η , our best estimate of the following excitation strength is $\eta' = \langle u \rangle - S(\langle u \rangle - \eta)$, where $\langle u \rangle$ is the average residual potential. Because $\langle u \rangle \approx 0$, we set $\eta' = -S(-\eta)$. The optimal value of η was found numerically, by minimizing the variation of fidelity over a range of gates acting on test states (see Results).

Application of a gate G requires no additional node of the network, only manipulation of the weights between the embedding and projecting parts. In simplest case these are directly set to

$$W_G = ALA^{-1} = G.$$

We have found however, that within some limits, the mechanism of *synaptic averaging* may provide improvement of the performance. In real networks, a single synapse contributes only a tiny fraction of the total input signal [2]. Multiple connections of similar lengths lead to signal accumulation, different delays – to temporal averaging. In our toy-model, the first case is replaced by single, but strong connections, while for implementation of the latter we directly use several edges having different lengths with proportionally attenuated couplings. In the case of a single-qubit gate, of the several configurations tested, the best results were obtained with just two-step average $\tau_{\text{avr}} = 2$, hence, the connections were fixed at $W_{G,1} = W_{G,2} = \frac{1}{2}G$.

Results. In order to reduce statistical uncertainties, all gates were tested on a fixed set of 14 pure states approximately evenly distributed on the Bloch sphere:

$$\left\{ |0\rangle, |1\rangle, \frac{1}{\sqrt{2}}(|0\rangle + e^{ik\pi/2}|1\rangle), \frac{\sqrt{\sqrt{3} \pm 1}|0\rangle + e^{i(2k+1)\pi/4}\sqrt{\sqrt{3} \mp 1}|1\rangle}{\sqrt{2\sqrt{3}}}, k \in \mathbb{Z}_4. \right\}$$

While the input nodes were fed with spike trains $\{X^A, X^B\}$ of joint probability distributions $\hat{p}_{\text{in}} \in \Omega_0^2$ corresponding to the above states, the output $\{X^{A'}, X^{B'}\}$ was tested for its coherence R , and fidelity with the desired distribution $G\hat{p}_{\text{in}}$. The initial test runs were made for several gates including Hadamard's, NOT, the antipode (non-unitary), and two rotations: $U_\theta = \exp(i\theta\hat{\sigma}_2/2)$, and $U_\phi = \exp(i\phi\hat{\sigma}_3/2)$. For the representative, the phase gate U_ϕ was selected – the effects of other operations were quantitatively similar, or better. Its representation $G_\phi = AL_\phi A^{-1}$, acting in Ω^2 reads

$$G_\phi = \frac{1}{2} \begin{pmatrix} 1 + \cos \phi & 1 - \cos \phi & -\sin \phi & \sin \phi \\ 1 - \cos \phi & 1 + \cos \phi & \sin \phi & -\sin \phi \\ \sin \phi & -\sin \phi & 1 + \cos \phi & 1 - \cos \phi \\ -\sin \phi & \sin \phi & 1 - \cos \phi & 1 + \cos \phi \end{pmatrix}.$$

The results presented in Fig. 2 are averages over 36 rotation angles evenly spaced across the entire interval $[0, 2\pi)$. The best performance was observed for $\phi = 0$ (identity) and $\phi = \pi$, while the worst cases were encountered around $\phi \approx \pm\pi/2$ (but not exactly at these angles). For each setting (σ, γ) , the inhibition level η was adjusted to minimize the variance of fidelity across the test states and rotation angles (cf. Fig. 2-insets). Note that while this optimization was mainly coincident with maximization of the fidelity itself, the trend in coherence was typically opposite. Had we chosen to optimize for purity of states ($R \rightarrow 1$), the figures would look different.

The prominent feature of Fig. 2a, is the overcoherence of output states in the limit $\gamma \rightarrow 0$. This means these distributions are too sharp to represent quantum states, and any subsequent application of another gate would certainly lead to a loss of accuracy. Interestingly, the average fidelity remains at relatively high level. This suggests a possibility of correcting the distributions by rescaling about the average. On the other hand, the fidelity SD is significant for small saturations, and becomes comparable with statistical uncertainties only above $\gamma \gtrsim 1$.

The conclusion drawn from Fig. 2b is clear: the circuit considered here is designed to work in deterministic regime $\sigma \rightarrow 0$. This makes an interesting contrast between stochastic nature of quantum states and the determinism of gates acting on them. As we are going to show, this dichotomy is not limited to the 1-qubit gate, but persists also in the case of entangling operation CNOT.

Finally, we have sought for an estimate of the time needed to complete the quantum rotations with this gate. Apart from the spatial resources, measured in terms of cells and connections being used, time is an important factor contributing to the overall cost of the realization. To assess this property, we have run the circuit while varying the *signal length* τ_{sig} : After an initial transient of $\tau_{\text{gate}} = 4 + \tau_{\text{avr}}$, the network was ran for $\tau_{\text{sig}} \geq 1$ successive steps, after which the cells were re-set to their initial state ($u^i = 0, X^i = 0$), ensuring that all

memory traces stored in residual potentials were erased. This procedure was repeated until satisfactory statistics ($N\tau_{\text{sig}} \approx 10^4$) was gathered.

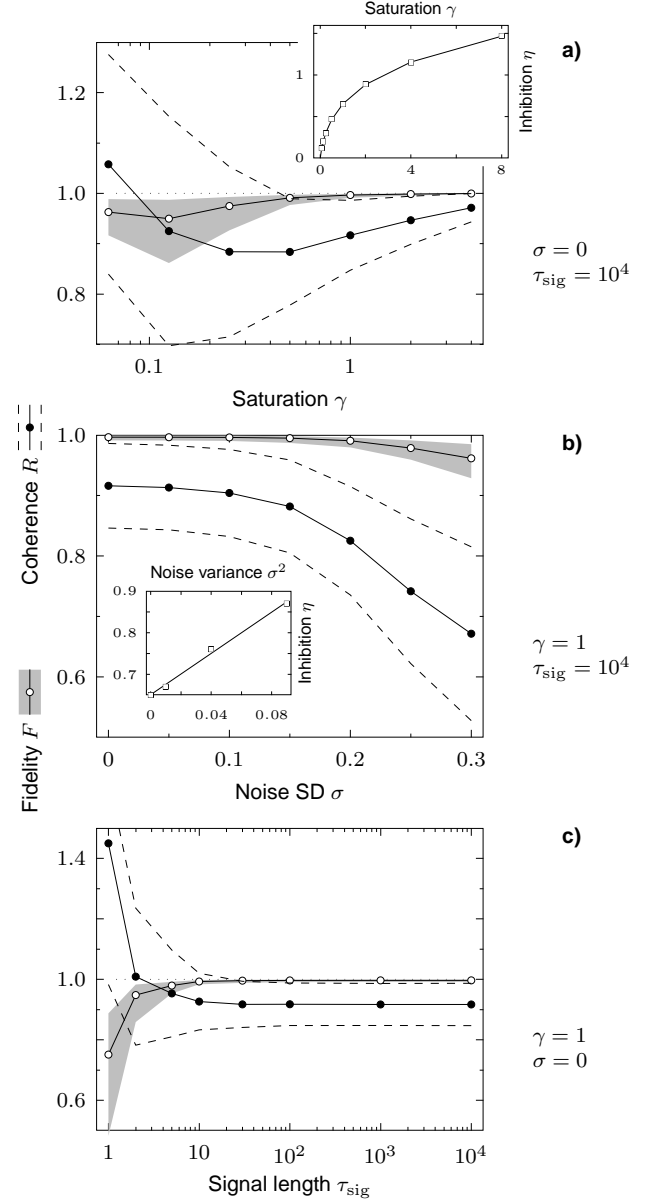


Figure 2 Performance of the 1-qubit phase gate in function of **a)** saturation level of the residual potential, **b)** noise SD of the activation function P , **c)** length of the input signal (note the scale difference between graphs). Synaptic averaging was fixed at $\tau_{\text{avr}} = 2$. Each point is a mean over 36 rotation angles within the whole interval $[0, 2\pi)$, and 14 pure states on which the phase gate was tested. With statistics of 10^4 steps per setting, the associated uncertainties are negligible – shaded regions (F) and broken lines (R) represent the standard deviations across the states and rotation angles. **Insets:** The inhibition levels used during simulations, optimized for minimization of the fidelity variance.

The results provided in Fig. 2c evidently show that the real temporal cost is not only the delay τ_{gate} , but a significant number of further steps are needed to ‘tune’ this gate to a signal. After approximately $\tau_{\text{sig}} \approx 30$ events the output quality no longer improves, and consequently one can identify τ_{sig} with the statistics needed for maximal efficiency. Since the latter is a function of

saturation γ and noise σ , one expects τ_{sig} to raise monotonically with γ and decrease as σ increases. In particular, the ideal case $\gamma \rightarrow \infty, \sigma \rightarrow 0$ would also require infinite statistics to achieve the best performance. One therefore finds yet another reason for the low saturation values: The finiteness of signals encoded in spike trains, limits the attainable efficiency of transformations, and high saturation values cannot provide improvement beyond these limitations.

4.2 The CNOT gate

Unlike the single-qubit gates which can, by means of a special choice of the POVM, be transformed to a permutation, the CNOT operation does not admit such representation⁴. With A given by (6), its operator $G_{\text{CNOT}} = AL_{\text{CNOT}}A^{-1}$ has the following structure

$$G_{\text{CNOT}} = \begin{pmatrix} H_1 - J_1 & H_1^\top + J_2 & H_2 & H_2^\top \\ H_1^\top + J_2 & H_1 - J_1 & H_2^\top & H_2 \\ -H_2 & -H_2^\top & H_1 - J_2 & H_1^\top + J_1 \\ -H_2^\top & -H_2 & H_1^\top + J_1 & H_1 - J_2 \end{pmatrix},$$

where

$$H_1 = \frac{1}{4} \begin{pmatrix} 1 & \frac{1}{\sqrt{3}} & 1 & \frac{1}{\sqrt{3}} \\ -\frac{1}{\sqrt{3}} & 1 & -\frac{1}{\sqrt{3}} & 1 \\ 1 & \frac{1}{\sqrt{3}} & 1 & \frac{1}{\sqrt{3}} \\ -\frac{1}{\sqrt{3}} & 1 & -\frac{1}{\sqrt{3}} & 1 \end{pmatrix},$$

$$H_2 = \frac{1}{4} \begin{pmatrix} \frac{1}{\sqrt{3}} & -1 & -\frac{1}{\sqrt{3}} & 1 \\ 1 & \frac{1}{\sqrt{3}} & -1 & -\frac{1}{\sqrt{3}} \\ -\frac{1}{\sqrt{3}} & 1 & \frac{1}{\sqrt{3}} & -1 \\ -1 & -\frac{1}{\sqrt{3}} & 1 & \frac{1}{\sqrt{3}} \end{pmatrix},$$

$$J_1 = \frac{1}{\sqrt{3}} \begin{pmatrix} 1 & 0 & 0 & 0 \\ 0 & 0 & 0 & -1 \\ 0 & 0 & 1 & 0 \\ 0 & -1 & 0 & 0 \end{pmatrix},$$

$$J_2 = \frac{1}{\sqrt{3}} \begin{pmatrix} 0 & 0 & 1 & 0 \\ 0 & -1 & 0 & 0 \\ 1 & 0 & 0 & 0 \\ 0 & 0 & 0 & -1 \end{pmatrix}.$$

As already mentioned, the POVM (6) has been chosen to optimize the CNOT gate. Indeed, the linear projection $\Pi : \Omega^4 \rightarrow \mathcal{V}_*^4$,

$$W_\Pi = \begin{pmatrix} 0 & 0 & 0 & 0 & 0 & \dots & 1 & 1 \\ 0 & 0 & 0 & 0 & 1 & \dots & 1 & 1 \\ 0 & 0 & 1 & 1 & 0 & \dots & 1 & 1 \\ 0 & 1 & 0 & 1 & 0 & \dots & 0 & 1 \end{pmatrix},$$

when combined with G_{CNOT} , shows the two pbits X^A and X^D are invariant under G_{CNOT} . These can be directly copied to the output $X^{A'}, X^{D'}$, as shown in Fig. 3. For that same reason, while implementing the embedding part Π^{-1} , we pair $\{X^A, X^D\}, \{X^B, X^C\}$, rather

than using the natural order $\{X^A, X^B\}, \{X^C, X^D\}$. The section Π^{-1} is a two-stage procedure: First, with the same construction as in 1-qubit case we separately embed the two marginals $\{X^A, X^D\}$ and $\{X^B, X^C\}$:

$$\Pi_I^{-1} : \mathcal{V}_*^4 \rightarrow \Omega^2 \times \Omega^2.$$

Next, we combine these into a single map

$$\Pi_{\text{II}}^{-1} : \Omega^2 \times \Omega^2 \rightarrow \Omega^4.$$

Since this is done with a linear mapping, there is again a rectifying feedback $W_{\text{rec,II}}$ obtainable from Eq. (7) applied to Π_{II} on Ω^4 . In contrast to Π_I^{-1} , the second-stage embedding Π_{II}^{-1} turns out to be unstable against noise, and the normalization feedback is now a necessity. Because of

$$\forall_i 2^{-4} \sum_j [W_{\text{rec,II}}]_{ij}^i = -\frac{9}{16}S(-1),$$

the normalization weights are set to

$$W_{\text{nor,II}} = -9S(-1)(-D_4 \oplus 1),$$

where $[D_4]_{ij}^i \equiv 2^{-4}$ is the diffusion operator, and '1' refers to the unit vertex \hat{v}_1 .

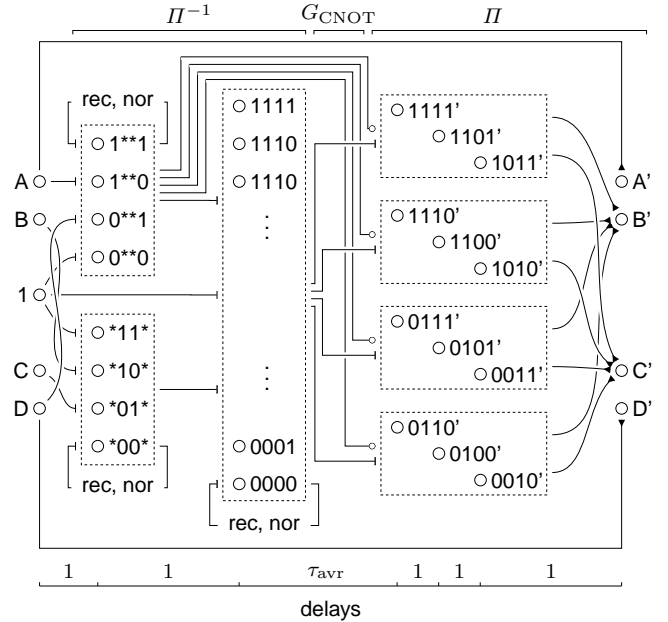


Figure 3 Schematic of the CNOT gate. The circuit has 38 nodes, and 1309 edges if the synaptic averaging is set to $\tau_{\text{avr}} = 4$. The transient time is $\tau_{\text{gate}} = 5 + \tau_{\text{avr}}$.

Thanks to the invariance of two pbits $X^{A'} = X^A, X^{D'} = X^D$, the hierarchical projection Π have been significantly simplified (in comparison to what is needed for general 2-qubit gate). The four partial projections from G_{CNOT} , shown on the right hand side of Fig. 3, are modulated directly by the marginal $\Pi_I^{-1}(X^A, X^D)$. The

⁴Would it be possible, then either the gate could have no entangling capability, or the marginal probabilities of the two qubits be not conserved.

mechanism of this modulation is the same as explained before (inhibition followed by attenuated excitation) and the same parameter η is set common on those connections.

Finally, the gate edges were multiplied, in order to use the synaptic averaging mechanism. We found no dramatic improvement while varying the averaging length τ_{avr} , at $\gamma \gtrsim 1$, nevertheless the performance was significantly better for small values of the saturation parameter. At $\gamma = 1$ the optimal length was $\tau_{\text{avr}} = 4$.

Results. The performance was assessed upon a testing set of 28 pure states, which included both separable and entangled ones:

$$\begin{aligned} & \{|00\rangle, |01\rangle, |10\rangle, |11\rangle, \\ & \frac{1}{\sqrt{2}}(|00\rangle + e^{ik\pi/2}|01\rangle), \quad \frac{1}{\sqrt{2}}(|00\rangle + e^{ik\pi/2}|10\rangle), \\ & \frac{1}{\sqrt{2}}(|00\rangle + e^{ik\pi/2}|11\rangle), \quad \frac{1}{\sqrt{2}}(|01\rangle + e^{ik\pi/2}|10\rangle), \\ & \frac{1}{\sqrt{2}}(|01\rangle + e^{ik\pi/2}|11\rangle), \quad \frac{1}{\sqrt{2}}(|10\rangle + e^{ik\pi/2}|11\rangle)\}, \end{aligned} \quad k \in \mathbb{Z}_4.$$

Interestingly, although some of these states are ‘preferred’ in terms of achieved fidelity F , there was no correlation between this measure and the entanglement property. This observation should not be surprising, because the mapping of 2-qubit states into joint probability distributions does not make entangled states distinct. It follows that even imperfect gate implementation should not distinguish these states from separable ones.

The results of simulations are presented in Fig. 4. Like before, for each setting of the control parameters (γ, σ) , the inhibition level η was adjusted to minimize the variance of fidelity across the test states.

Qualitatively, the figures 4 are largely similar to what had been obtained for 1-qubit gates (Fig. 2), the major difference is in the range of achieved fidelities and output coherences. Standard deviations of coherence R increased evenly by approximately a factor of 2, while the fidelity SD multiplied by about 4 – 5. The most dramatic changes are observed in Fig. 4a: Whereas at low saturation values ($\gamma < 1$) the 1-qubit gate worked relatively well, in the case of CNOT a huge overcoherence takes place along with significant fidelity loss.

For a reasonable performance at $\sigma = 0$ and $\tau_{\text{sig}} \gtrsim 30$ one needs $\gamma \gtrsim 1$. In this regime one finds $F \gtrsim 0.97$ ($-0.03, +0.02$), corresponding to the unitary error $\alpha \lesssim 14^\circ$ ($-5, +4$); with noise at $\sigma = 0.3$ and $\gamma = 1$ the fidelity drops down to $F = 0.77$ ($-0.11, +0.15$), or $\alpha = 42^\circ$ ($-22, +12$), what is hardly acceptable for a large-scale quantum computation. While comparing these values with the best to-date experimental achievements ($F \sim 0.7 - 0.8$ with trapped ions [13], $F \sim 0.6 - 0.8$ with Josephson junctions [14], $F \sim 0.85$ in optical setup [15]) one has to take into account the many simplifications of our toy-model. More realistic simulations, or ultimately – realizations, may not necessarily prove as good as this one, and would probably require additional resources to

implement some of the error correcting schemes, nevertheless the principle of quantum computing with neural networks has been demonstrated.

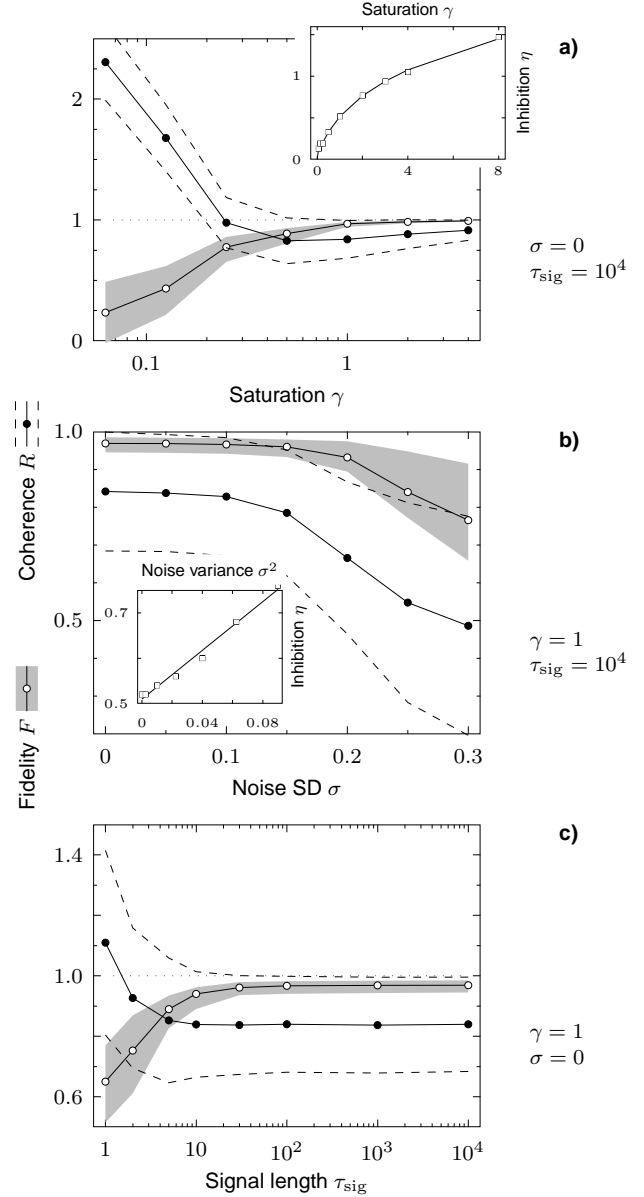


Figure 4 Performance of the CNOT gate for synaptic averaging fixed at $\tau_{\text{avr}} = 4$. Note the differences in ranges, while comparing with Fig. 2. The statistics for each setting is 10^4 steps, and each point is an average over 28 test states.

5 Discussion

We have studied the potential of an artificial neural network to operate on correlated spike trains assuming the latter to encode quantum states. The model neurons are reduced here down to the essential ingredients of computational capability. Few comments concerning the simplifications made are in order at this point:

First, we have completely neglected the synaptic noise, by assuming the signals to be relayed undisturbed between cells. The justification is that here the few edges of each node represent averages over $10^3 - 10^4$ real

synaptic connections therefore the impact of faulty transmission through a single synapse is greatly reduced. But inclusion of this likely source of errors may still be a significant factor reducing the overall performance.

Second, the time duration of processed signals are assumed to be much shorter than the synaptic plasticity scale. Adaptation is an inherent element of information processing in the brain, but it conflicts with the objective of reliable signal transformations in that there is a trade-off between computing efficiency and adaptive capability. The resolution is provided by separation in time scales between the two processes – transformations act over short signals, typically in response to rapidly varying external stimuli. This is consistent with the optimal signal length which was found here for both 1- and 2-qubit gates to be of order ~ 30 steps. Assuming the time step is set to ~ 5 ms leads to a realistic signal duration of ~ 150 ms.

Third, the detrimental effect of cellular noise on the performance of quantum gates clearly shows the deterministic regime to be preferable at least for the coding scheme considered here. On one hand, a sharp firing threshold needed for the neurons to act as ‘counters’ which discretize linearly accumulated input signals, corroborates with the theoretical analysis of optimality in terms of information encoding [21]. But on the other, the noise itself which blurs this threshold has been shown to be a viable resource acting through the mechanisms of stochastic resonance [22]. This suggests to consider alternative quantum coding schemes, which would make use of the inherent uncertainty in spike generation, provided the relevant conditions are stable enough (*e.g.*, noise variance at a constant, moderate level).

It is worthwhile to note at this point, that the quantum states are not absolute entities, and the same set of spike trains may be ‘quantized’ in many different ways depending on the assumed definition of a state. Accordingly, the quantum transformations as well as their implementations will differ. We have discussed here only two coding schemes (referred to as the ‘dense’ and ‘sparse’ spatial code), but it appears plausible, that the real networks may actually alternate (or combine) many different encodings, depending on the nature of the input signal and the functional properties of the circuit. An evident possibility is the *sparse temporal code* based on probability waves, particularly attractive for at least two reasons: First, the brain waves provide the frequency basis necessary for phase discrimination, and there is an experimental indication for independence between rate and phase variables [23]. The question is not whether the spiking probability oscillation does have a role, but rather what is the relevant number of modes involved in computation (if more than two then one should consider qudits instead of just qubits). Second, while the ‘dense’ code requires two random binary variables per qubit, by trading spatial for temporal resources, probability waves allow to encode one-qubit per neuron. The

drawback is that the mechanisms of short term synaptic plasticity [18–20] makes the neural circuits operating on this form of a code susceptible to unwanted modifications [30]. From this perspective, the use of sparse spatial coding [24–29], appears to be advantageous, since such spike trains have by definition no temporal correlations, and hence the circuits operating in this fashion are expected to be more stable.

In summary, we have demonstrated the principle of employing quantum coding in artificial neural networks, by providing examples of circuits which realize quantum gates. There is a room for improvement and further investigation with more realism put into the model, alternative circuits, and algorithm implementations. Exploring the possible ways in which neural networks can handle quantum codes, can certainly benefit both the quantum mechanics and neuroscience. On one hand, applications of QM to neural systems broaden the range of possibilities to be considered when seeking to understand the language of spikes, on the other – macroscopic realizations can provide clues about the microscopic phenomena upon which QM originated.

References

- [1] F. Rieke, D. Warland, R.R. de Ruyter van Steveninck, W. Bialek, *“Spikes: Exploring the Neural Code”*, The MIT Press, Cambridge, Massachusetts 1997.
- [2] P.S. Churchland, T.J. Sejnowski, *“The Computational Brain”*, The MIT Press, Cambridge, Massachusetts 1992.
- [3] D. Aerts, *“A possible explanation for the probabilities of quantum mechanics”*, *J. Math. Phys.* **27** (1986), 202–210.
- [4] D. Aerts, M. Czachor, *“Bag-of-words problem and semantic analysis in Fock space”*, [quant-ph/0309022](https://arxiv.org/abs/quant-ph/0309022)
- [5] D.C. Brody, *“Shapes of quantum states”*, *J. Phys. A: Math. Gen.* **37** (2004), 251–257.
- [6] L.E. Ballentine, *“The statistical interpretation of quantum mechanics”*, *Rev. Mod. Phys.* **42:2** (1970), 358–381.
- [7] A. Peres, *“Quantum Theory: Concepts and Methods”*, Kluwer Academic Publishers, Dordrecht 1995.
- [8] A. Peres, D.R. Terno, *“Convex probability domain of generalized quantum measurements”*, *J. Phys. A* **31** (1998), L671–L675.
- [9] C.M. Caves, Ch.A. Fuchs, R. Schack, *“Quantum probabilities as Bayesian probabilities”*, *Phys. Rev. A* **65** (2002), 022305.
- [10] V. Bužek, M. Hillery, R.F. Werner, *“Optimal manipulations with qubits: Universal-NOT gate”*, *Phys. Rev. A* **60** (1999), R2626–9.
- [11] F. De Martini, V. Bužek, F. Sciarrino, C. Sias, *“Experimental realization of the quantum universal NOT gate”*, *Nature* **419** (2002), 815–818.
- [12] A. Barenco, C.H. Bennett, R. Cleve, D.P. DiVincenzo, N. Margolus, P. Shor, T. Sleator, J.A. Smolin, H. Weinfurter, *“Elementary gates for quantum computation”*, *Phys. Rev. A* **52** (1995), 3457–3467.
- [13] F. Schmidt-Kaler, *et al.* *“Realization of the Cirac-Zoller controlled-NOT quantum gate”*, *Nature* **422** (2003), 408–411.
- [14] T. Yamamoto, Yu.A. Pashkin, O. Astafiev, Y. Nakamura, J.S. Tsai, *“Demonstration of conditional gate operation using superconducting charge qubits”*, *Nature* **425** (2003), 941–946.
- [15] J.L. O’Brien, G.J. Pryde, A.G. White, T.C. Ralph, *“Demonstration of an all-optical quantum controlled-NOT gate”*, *Nature* **426** (2003), 264–267.
- [16] M. Carandini, D. Heeger, J.A. Movshon, *“Linearity and normalization in simple cells of the macaque primary visual cortex”*, *J. Neurosci.* **17** (1997), 8621–8644.

- [17] G.G. Turrigiano, K.R. Leslie, N.S. Desai, L.C. Rutheford, S.B. Nelson, "Activity-dependent scaling of quantal amplitude in neocortical neurons", *Nature* **391** (1998), 892–896.
- [18] H. Markram, J. Lubke, M. Frotscher, B. Sakmann, "Regulation of synaptic efficacy by coincidence of postsynaptic SPs and EPSPs", *Science* **275** (1997), 213–215.
- [19] G.Q. Bi, M.M. Poo, "Synaptic modifications in cultured hippocampal neurons: dependence on spike timing, synaptic strength, and postsynaptic cell type", *J. Neurosci.* **18** (1998), 10464–10472.
- [20] R.C. Froemke, Y. Dan, "Spike-timing-dependent synaptic modification induced by natural spike trains", *Nature* **416** (2002), 433–438.
- [21] M. Bethge, D. Rotermund, K. Pawelzik, "Optimal neural rate coding leads to bimodal firing rate distributions", *Network: Comput. Neural Syst.* **14** (2003), 303–319.
- [22] L. Gammaitoni, P. Hänggi, P. Jung, F. Marchesoni, "Stochastic resonance", *Rev. Mod. Phys.* **70** (1998), 223–287.
- [23] J. Huxter, N. Burgess, J. OKeefe, "Independent rate and temporal coding in hippocampal pyramidal cells", *Nature* **425** (2003), 828–832.
- [24] D.J. Field, "Relations between the statistics of natural images and the response properties of cortical cells", *J. Opt. Soc. Am. A* **4** (1987), 2379–2394.
- [25] C.A. Barnes, B.L. McNaughton, S.J. Mizumori, B.W. Leonard, L.H. Lin, "Comparison of spatial and temporal characteristics of neuronal activity in sequential stages of hippocampal processing", *Prog. Brain Res.* **83** (1990), 287–300.
- [26] B.A. Olshausen, D.J. Field, "Emergence of simple-cell receptive field properties by learning a sparse code for natural images", *Nature* **381** (1996), 607–609.
- [27] A. Arieli, A. Sterkin, A. Grinvald, A. Aertsen, "Dynamics of ongoing activity: Explanation of the large variability in evoked cortical responses", *Science* **273** (1996), 1868–1871.
- [28] A.J. Bell, T.J. Sejnowski, "The "independent components" of natural scenes are edge filters", *Vision Res.* **37** (1997), 3327–3338.
- [29] T. Kenet, D. Bibitchkov, M. Tsodyks, A. Grinvald, A. Arieli, "Spontaneously emerging cortical representations of visual attributes", *Nature* **425** (2003), 954–956.
- [30] A.L. Fairhall, G.D. Lewen, W. Bialek, R.R. de Ruyter van Steveninck, "Efficiency and ambiguity in an adaptive neural code", *Nature* **412** (2001), 787–792.